Journal of Petroleum Science and Engineering 108 (2013) 342–351

Contents lists available at ScienceDirect

Journal of Petroleum Science and Engineering

journal homepage: www.elsevier.com/locate/petrol

# A 3D hybrid element-based finite-volume method for heterogeneous and anisotropic compositional reservoir simulation

Francisco Marcondes [a], Luiz Otávio Schmall Santos [b], Abdoljalil Varavei [b], Kamy Sepehrnoori [b,*]

[a] Department of Metallurgical Engineering and Material Science, Federal University of Ceará, Fortaleza, Ceará, Brazil
[b] Petroleum and Geosystems Engineering Department, The University of Texas at Austin, 1 University Station C0300, Austin, TX 78712-0228, USA

ARTICLE INFO

*Article history:*
Received 16 October 2012
Accepted 28 April 2013
Available online 14 May 2013

*Keywords:*
3D unstructured hybrid grids
isothermal compositional reservoir simulation
element-based finite-volume method
anisotropic and heterogeneous reservoir simulation

ABSTRACT

3D unstructured grids for heterogeneous and anisotropic compositional reservoir simulation in conjunction with an element-based finite-volume method (EbFVM) are presented. The approximate equations of the EbFVM adopted in this work are obtained from integration of the compositional material balance equations directly to each element type. Using this approach, the final approximation equations do not impose any limitation on the element shape. The methodology used in this work is suitable for modeling complex features of reservoirs such as irregular boundaries, fractures, faults, inclined and distorted wells. The mesh for 3D dimensional domains can be built of hexahedrons, tetrahedrons, pyramids and prisms, or a combination of these elements. According to the number of vertices, each element is divided into sub-elements and then mass balance equations for each component are integrated along each interface of the sub-elements. The finite-volume conservation equations are assembled from the contribution of all the elements that share a vertex creating a cell vertex approach. It is expected that the approach employed in this work will have less grid orientation effect than the one using Cartesian meshes since more gridblocks are used in the approximated equations. The results for several compositional reservoir simulation case studies are presented to demonstrate the application of the method.



## 1. Introduction

From discretization point of view, unstructured grids are more flexible than most grids employed in petroleum reservoir simulation (Cartesian and regular corner point meshes). The application of unstructured grids in petroleum reservoir simulation started about two decades ago by Forsyth (1990), Fung et al. (1991), and Gottardi and Dall´Olio (1992). The approach used by these authors is called Control Volume Finite Element Method (CVFEM). In these works, linear triangle elements were used in order to obtain the material balance equation for 2D reservoirs. The approximate equations for single-phase flow were multiplied by the phase mobilities in order to obtain the approximate equations for multi-component/multiphase flows. Edwards (2000, 2002) presented the multipoint-flux approximation for 2D discretization using triangle and quadrilateral elements. Verma and Aziz (1997) used the multipoint-flux approximation for the discretization of 3D geometries in conjunction with tetrahedron element. In the multipoint-flux approximation, all physical properties including the porosity and the absolute permeability tensor are stored at the vertex of the elements. In this approach, a local linear system involving the potential at the interfaces and in the vertex of the elements needs to be solved. Also, using the unstructured mesh, several authors have employed the finite-element or the mixed finite element methods in petroleum reservoir simulation. Hegre et al. (1986) used quadrilateral elements in conjunction with the finite element method to investigate the grid orientation effect. Deb et al. (1995) also employed the finite element method for the solution of water flooding problems in 2D and 3D reservoirs. Mixed finite element method has been investigated by Durlofsky and Chien (1993) and Hoteit and Firoozabadi (2005, 2006).

The ideas of Raw (1985) and Baliga and Patankar (1983) were used by Cordazzo (2004) and Cordazzo et al. (2004a, 2004b) for solving water flooding problems. Although the final approximate equations are similar to the ones obtained through the CVFEM methodology, they derive the approximate equations starting from the multi-component/multiphase flow. The authors demonstrated that the equations obtained from a single-phase flow equation and then multiplied by phase mobilities do not correctly approximate the equations for multiphase flow. According to Forsyth (1990) and Fung et al. (1991), the distortion angle of the grid needs to be equal or less than right angle, in order to avoid negative transmissibilities.

* Corresponding author. Tel.: +1 512 417 231; fax: +1 512 471 0231.
*E-mail address:* kamys@mail.utexas.edu (K. Sepehrnoori).

0920-4105/$ - see front matter © 2013 Elsevier B.V. All rights reserved.
http://dx.doi.org/10.1016/j.petrol.2013.04.024

Cordazzo (2004) and Cordazzo et al. (2004a, 2004b) called their methodology element-based finite volume method (EbFVM). As explained by Maliska (2004), we have a methodology that still follows the conservative principles at the discrete level and only borrows the idea of elements and shape functions from the finite element method. Therefore, the term EbFVM seems to be more appropriate than CVFEM used by other authors and this terminology will also be used in the present paper. Cordazzo (2004) applied an implicit pressure explicit saturation (IMPES) formulation in conjunction with highly distorted triangular and quadrilateral elements with EbFVM to simulate two-phase fluid flow (oil and water) problems. Excellent results were obtained with very little grid orientation effects. As mentioned by Marcondes and Sepehrnoori (2007, 2010), this restriction can be difficult to follow for most reservoirs due mainly to the heterogeneity of the medium, fractures, faults, or even irregular boundaries of the reservoirs. These authors applied the EbFVM to simulate compositional, multiphase, multi-component fluid-flow problems in conjunction with anisotropic and heterogeneous reservoirs. Although the meshes used for most of the investigations presented several elements with angles equal or bigger than right angles, the results obtained with triangles and quadrilateral presented a good agreement. Following a similar approach used by the other EbFVM papers, Paluszny et al. (2007) presented a fully 3D discretization using hexahedron, tetrahedron, prism, and pyramid elements. They applied their approach to simulate the water flooding problem in naturally fractured reservoirs.

In this study, we investigated the EbFVM in conjunction with 3D heterogeneous and anisotropic reservoirs using hexahedron, tetrahedron, prism, and pyramid elements. Except for absolute permeability tensor and porosity, all the physical parameters are evaluated at the vertices of each element rendering a cell vertex approach. We also assume that each element has constant porosity and permeability tensors, but the values of these properties can change from element to element. As each element has a constant permeability tensor, all the fluxes along each integration point employ the same absolute permeability. General Purpose Adaptive Simulator (GPAS) was developed at the Center for Petroleum and Geosystems Engineering at The University of Texas at Austin for the simulation of enhanced recovery processes. GPAS is a fully implicit, multiphase/multi-component simulator which can handle the simulation of several enhanced oil recovery processes. This simulator is divided into two main modules: Framework and EOScomp. Framework is responsible for input/output and memory allocation, while EOScomp handles the computations for flash calculation and solution of non-linear equations arising from the discretization of the governing equations. Details for EOScomp and Framework modules can be found in Wang et al. (1997) and Parashar et al. (1997), respectively.

## 2. Governing equations

Isothermal, multi-component, multiphase fluid flow in a porous medium can be described using three types of equations: the component-material balance equation, the phase equilibrium equation, and the equation for constraining phase saturations and component concentrations (Wang et al., 1997).

The material balance equation for the $i$-th component for a full symmetric permeability tensor using the Einstein notation can be written as

$$\frac{\partial(\phi N_i)}{\partial t}-\nabla\cdot\left[\sum_{j=1}^{n_p}\xi_j x_{ij}\lambda_j\overline{\overline{K}}\cdot\nabla\Phi_j\right]-\frac{q_i}{V_b}=0;\quad i=1,\,2,..,\,n_{c+1}. \tag{1}$$

In Eq. (1), $n_{c+1}$ denotes the number of hydrocarbon components plus the water component, $n_p$ is the number of phases present in the reservoir, $\phi$ is the porosity, $N_i$ is the moles of the $i$-th component per unit of pore volume, $\xi_j$ and $\lambda_j$ are the molar density and the relative mobility of the $j$-th phase respectively, $x_{ij}$ is the molar fraction of the $i$-th component in the $j$-th phase, $\overline{\overline{K}}$ is the absolute permeability tensor, and $V_b$ is the volume of control-volume that contains a well. $\Phi_j$ is the potential of the $j$-th phase and is given by

$$\Phi_j=P_j-\gamma_j Z, \tag{2}$$

where $P_j$ denotes the pressure of the $j$-th phase and $Z$ is the depth, which is positive in the downward direction.

The first partial derivative of the total Gibbs free energy with respect to the independent variables gives the equality of component fugacities among all phases,

$$\begin{aligned} &f_i^g-f_i^o=0;\quad i=1,....,\,n_c\\ &f_i^{L_2}-f_i^o=0;\quad i=1,....,\,n_c. \end{aligned} \tag{3}$$

In Eq. (3), $f_i^j=\ln(x_{ij}\phi_{ij})$, where $\phi_{ij}$ is the fugacity coefficient of component $i$ in the $j$-th phase, $L_2$ denotes the second liquid phase, and $n_c$ is the number of components excluding the water. The restriction of the molar fraction is used to obtain the solution of Eq. (3),

$$\sum_{i=1}^{n_c}x_{ij}-1=0,\quad j=2,..,\,n_p;\qquad \sum_{i=1}^{n_c}\frac{z_i(K_i-1)}{1+\nu(K_i-1)}=0, \tag{4}$$

where $z_i$ is the overall molar fraction of the $i$-th component, $K_i$ is the equilibrium ratio for the $i$-th component, and $\nu$ is the mole fraction of the gas phase in the absence of water. The closure equation comes from the volume constraint, i.e., the available pore volume of each cell must be filled by all phases present in the reservoir. This constraint gives rise to the following equation:

$$V_b\sum_{i=1}^{n_c+1}(\phi N_i)\sum_{j=1}^{n_p}L_j\bar{v}_j-V_p=0, \tag{5}$$

where $V_p$ is the pore volume, $\bar{v}_j$ and $L_j$ are the molar volume of and the amount of the $j$-th phase, respectively. In GPAS the unknown primary variables are water pressure $P_w$, $N_1$,..., $N_{nc}$, ln $K_1$,..., ln $K_{nc}$. It is important to mention that in GPAS simulator water is always assumed to be present in the reservoir which is in agreement with the field cases.

## 3. Approximate equation

In the EbFVM, each element is divided into sub-elements. These sub-elements will be called sub-control volumes. The conservation equation, Eq. (1), needs to be integrated for each one of these sub-control volumes. Fig. 1 presents the four elements employed and the sub-control volumes associated with each element. Fig. 1 shows that except for pyramid, each element has three quadrilateral integration surfaces associated with each sub-control volume. For the pyramid element, the sub-control volumes associated with the base have two triangular integration surfaces and one quadrangular integration surface, and the sub-control volume associated with the apex has four quadrilateral integration surfaces. It is worthwhile to mention that in general, due to the shape functions, the hexahedron element should be used for most parts of the reservoir. Due to the largest number of vertices of hexahedron element, the final approximate equation of this element will involve much more vertices than any one of the-other elements. In general, if a regular hexahedron mesh is employed the stencil for the internal vertices will involve 27 vertices, which is much larger than the seven vertices when Cartesian meshes are employed. For areas needing a local grid refinement, tetrahedron element is the most indicated. For areas between hexahedron and tetrahedron elements, transition elements like pyramids or prisms are necessary in order to match the

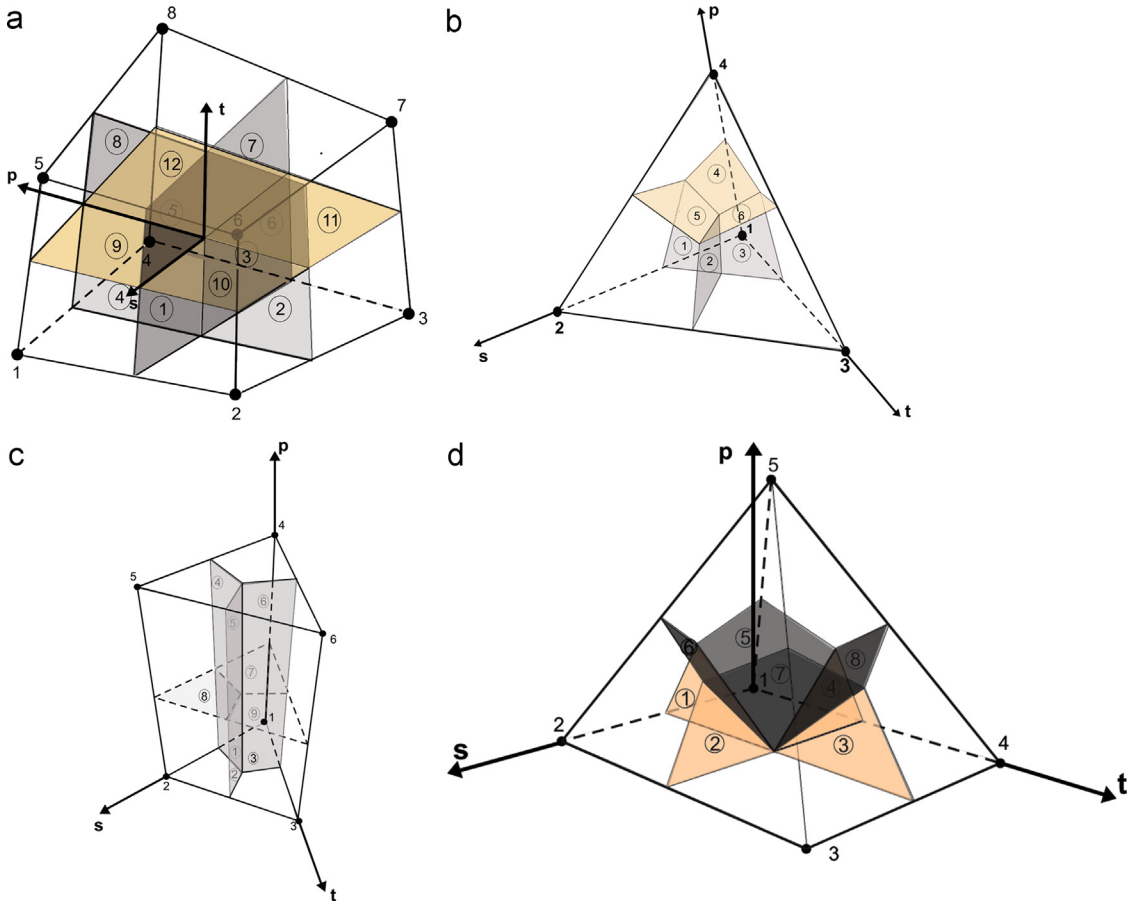


**Fig. 1.** 3D elements and their respective sub-control volumes: (a) hexahedron, (b) tetrahedron, (c) prism, and (d) pyramid.

triangular surfaces of tetrahedron and quadrilateral surfaces of the hexahedrons. Integrating Eq. (1) in time and for each one of the sub-control volumes and applying the Gauss theorem for the advective term we obtain

$$\int_V \frac{\partial(\phi N_i)}{\partial t} dV - \int_A \sum_{j=1}^{n_p} \xi_j x_{ij} \lambda_j \overline{\overline{K}} \cdot \nabla \Phi_j \cdot \overrightarrow{dA} - \int_V \frac{q_i}{V_b} = 0; \quad i = 1,\ 2,..,\ n_{c+1}. \tag{6}$$

To evaluate the first and second terms of Eq. (6), it is necessary to define the shape functions. The shape functions used for hexahedron, tetrahedron, prism, and pyramid elements are correspondingly defined by Eqs. (7)–(10).

$$N_1(s,t,p) = \frac{(1+s)(1-t)(1+p)}{8}; \quad N_2(s,t,p) = \frac{(1+s)(1-t)(1-p)}{8}$$
$$N_3(s,t,p) = \frac{(1-s)(1-t)(1-p)}{8}; \quad N_4(s,t,p) = \frac{(1-s)(1-t)(1+p)}{8}$$
$$N_5(s,t,p) = \frac{(1+s)(1+t)(1+p)}{8}; \quad N_6(s,t,p) = \frac{(1+s)(1+t)(1-p)}{8}$$
$$N_7(s,t,p) = \frac{(1-s)(1+t)(1-p)}{8}; \quad N_8(s,t,p) = \frac{(1-s)(1+t)(1+p)}{8}, \tag{7}$$

$$N_1(s,t,p) = 1-s-t-p; \quad N_2(s,t,p) = s$$
$$N_3(s,t,p) = t; \quad N_4(s,t,p) = p, \tag{8}$$

$$N_1(s,t,p) = (1-s-t)(1-p); \quad N_2(s,t,p) = s(1-p)$$
$$N_3(s,t,p) = t(1-p); \quad N_4(s,t,p) = p(1-s-t), \tag{9}$$
$$N_5(s,t,p) = sp; \quad N_6(s,t,p) = tp$$

$$N_1(s,t,p) = \frac{1}{4}\left[(1-s)(1-t)-p+stp/(1-p)\right]$$
$$N_2(s,t,p) = \frac{1}{4}\left[(1+s)(1-t)-p-stp/(1-p)\right]$$
$$N_3(s,t,p) = \frac{1}{4}\left[(1+s)(1+t)-p-stp/(1-p)\right]$$
$$N_4(s,t,p) = \left[(1-s)(1+t)-p-stp/(1-p)\right]$$
$$N_5(s,t,p) = p \tag{10}$$

In Eqs. (7)–(10) $s$, $t$, and $p$ denote the local axes in the transformed domain. For the hexahedron element each of these axes varies from −1 to 1. For the other elements the variation is from 0 to 1. In order to obtain the shape functions for the hexahedron element, we assumed a tri-linear variation of the physical properties with $x$, $y$, and $z$. Similar approach can be performed for the other three elements. Each deformed element of the mesh (physical domain) can be represented by its regular element in the transformed domain presented in Fig. 1.

Using the shape functions, any physical properties or positions can be evaluated inside an element as

$$x(s,t,p) = \sum_{i=1}^{N_v} N_i x_i; \quad y(s,t,p) = \sum_{i=1}^{N_v} N_i y_i;$$
$$z(s,t,p) = \sum_{i=1}^{N_v} N_i z_i; \quad \Phi_j(s,t,p) = \sum_{i=1}^{N_v} N_i \Phi_{ji}, \tag{11}$$

where $N_v$ denotes the number of vertex for each element, and $N_i$ are the shape functions of each element. Elements using the same shape function for coordinates and physical properties are known as isoparametric elements (Hughes, 1987). Using the shape

functions, gradients of potentials can be easily evaluated as

$$\frac{\partial \Phi_j}{\partial x} = \sum_{i=1}^{N_v} \frac{\partial N_i}{\partial x}\Phi_{ji}; \quad \frac{\partial \Phi_j}{\partial y} = \sum_{i=1}^{N_v} \frac{\partial N_i}{\partial y}\Phi_{ji}; \quad \frac{\partial \Phi_j}{\partial z} = \sum_{i=1}^{N_v} \frac{\partial N_i}{\partial z}\Phi_{ji} \tag{12}$$

To evaluate the gradients, it is necessary to obtain the derivatives of the shape functions relative to $x$, $y$, and $z$. These derivatives are given by

$$\begin{aligned}
\frac{\partial N_i}{\partial x} &= \frac{1}{\det(J_t)}\left(\frac{\partial y}{\partial t}\frac{\partial z}{\partial p} - \frac{\partial y}{\partial p}\frac{\partial z}{\partial t}\right)\frac{\partial N_i}{\partial s} - \frac{1}{\det(J_t)}\left(\frac{\partial y}{\partial s}\frac{\partial z}{\partial p} - \frac{\partial y}{\partial p}\frac{\partial z}{\partial s}\right)\frac{\partial N_i}{\partial t} \\
&\quad + \frac{1}{\det(J_t)}\left(\frac{\partial y}{\partial s}\frac{\partial z}{\partial t} - \frac{\partial y}{\partial t}\frac{\partial z}{\partial s}\right)\frac{\partial N_i}{\partial p} \\
\frac{\partial N_i}{\partial y} &= -\frac{1}{\det(J_t)}\left(\frac{\partial x}{\partial t}\frac{\partial z}{\partial p} - \frac{\partial x}{\partial p}\frac{\partial z}{\partial t}\right)\frac{\partial N_i}{\partial s} + \frac{1}{\det(J_t)}\left(\frac{\partial x}{\partial s}\frac{\partial z}{\partial p} - \frac{\partial x}{\partial p}\frac{\partial z}{\partial s}\right) \\
&\quad \frac{\partial N_i}{\partial t} - \frac{1}{\det(J_t)}\left(\frac{\partial x}{\partial s}\frac{\partial z}{\partial t} - \frac{\partial x}{\partial t}\frac{\partial z}{\partial s}\right)\frac{\partial N_i}{\partial p} \\
\frac{\partial N_i}{\partial z} &= \frac{1}{\det(J_t)}\left(\frac{\partial x}{\partial t}\frac{\partial y}{\partial p} - \frac{\partial x}{\partial p}\frac{\partial y}{\partial t}\right)\frac{\partial N_i}{\partial s} - \frac{1}{\det(J_t)}\left(\frac{\partial x}{\partial s}\frac{\partial y}{\partial p} - \frac{\partial x}{\partial p}\frac{\partial y}{\partial s}\right)\frac{\partial N_i}{\partial t} \\
&\quad + \frac{1}{\det(J_t)}\left(\frac{\partial x}{\partial s}\frac{\partial z}{\partial t} - \frac{\partial x}{\partial t}\frac{\partial y}{\partial s}\right)\frac{\partial N_i}{\partial p}
\end{aligned} \tag{13}$$

where $\det(J_t)$ is the Jacobian determinant of the transformation and it is given by

$$\begin{aligned}
\det(J_t) &= \frac{\partial x}{\partial s}\left(\frac{\partial y}{\partial t}\frac{\partial z}{\partial p} - \frac{\partial y}{\partial p}\frac{\partial z}{\partial t}\right) - \frac{\partial x}{\partial t}\left(\frac{\partial y}{\partial s}\frac{\partial z}{\partial p} - \frac{\partial y}{\partial p}\frac{\partial z}{\partial s}\right) \\
&\quad + \frac{\partial x}{\partial p}\left(\frac{\partial y}{\partial s}\frac{\partial z}{\partial t} - \frac{\partial y}{\partial t}\frac{\partial z}{\partial s}\right).
\end{aligned} \tag{14}$$

Further details of the expressions given by Eq. (13) can be found in Maliska (2004). To perform the integral of Eq. (6), it is necessary to define the volumes of each sub-control volume and the area of each interface. The volumes of each sub-control volume for hexahedron, tetrahedron, prism, and pyramid elements are given by

Hexahedron:

$$Vscv_i = \det(J_t), \tag{15}$$

Tetrahedron:

$$Vscv_i = \det(J_t)/6, \tag{16}$$

Prism:

$$Vscv_i = \det(J_t)/12, \tag{17}$$

Pyramid:

$$Vscv_i = \begin{cases} 2\det(J_t)/9 & \text{for} \quad i = 1, \ldots, 4 \text{ (base)} \\ 4\det(J_t)/9 & \text{for} \quad i = 5 \text{ (apex)} \end{cases} \tag{18}$$

It is important to mention that $\det(J_t)$ needs to be evaluated at the center of each sub-control volume. The area of each interface for the hexahedron element is evaluated by

$$\begin{aligned}
\overrightarrow{dA} &= \left(\frac{\partial y}{\partial m}\frac{\partial z}{\partial n} - \frac{\partial y}{\partial n}\frac{\partial z}{\partial m}\right) dm\, dn\, \vec{i} - \left(\frac{\partial x}{\partial n}\frac{\partial z}{\partial m} - \frac{\partial x}{\partial m}\frac{\partial z}{\partial n}\right) dm\, dn\, \vec{j} \\
&\quad + \left(\frac{\partial x}{\partial m}\frac{\partial y}{\partial n} - \frac{\partial x}{\partial n}\frac{\partial y}{\partial m}\right) dm\, dn\, \vec{k},
\end{aligned} \tag{19}$$

where $m$ and $n$ denote the local system $s$, $t$, or $p$. For the other elements, the interfaces can be evaluated using a similar procedure. We just need to define the local vectors for each interface. Finally, it is important to mention that only half of the cross product is used for the triangular interfaces of the pyramid element.

Substituting Eqs. (15) through (18) for the accumulation term; and (19) and similar ones for the other elements of the advective flux into Eq. (6); and evaluating the fluid properties through a fully implicit procedure, the following equations for the accumulation ($Acc$) term and the advective flux ($F$) are obtained:

$$Acc_{m,i} = Vscv_{m,i}\left(\left(\frac{\phi N_m}{\Delta t}\right)_i - \left(\frac{\phi N_m}{\Delta t}\right)_i^o\right); \quad m = 1, \ldots, N_v; \quad i = 1, .., n_c, n_w, \tag{20}$$

$$F_{m,i} = \int_A \sum_{j=1}^{n_p} \xi_j x_{ij} \lambda_j \overline{\overline{K}} \cdot \nabla \Phi_j \cdot \overrightarrow{dA} = \int_A \sum_{j=1}^{n_p} \xi_j x_{ij} \lambda_j K_{nl} \frac{\partial \Phi_j}{\partial x_l} dA_n; \quad m = 1, \ldots, N_v; \quad n, l = 1, .., 3, \tag{21}$$

where the superscript $o$ denotes values from the previous time-step. By inspecting Eq. (21), it can be inferred that it is necessary to evaluate molar densities, molar fractions, and mobilities in three interfaces of each sub-control volume. To evaluate these properties, an upwind scheme based on Cordazzo et al. (2004) will be used. The mobilities and other fluid properties are evaluated at the integration point 1 of Fig. 1a, for instance, by

$$\begin{aligned}
\lambda_{j1} &= \lambda_{j2} \quad \text{if} \quad \overline{\overline{K}} \cdot \nabla \Phi_j \cdot \overrightarrow{dA}\,|_{ip1} \leq 0 \\
\lambda_{j1} &= \lambda_{j1} \quad \text{if} \quad \overline{\overline{K}} \cdot \nabla \Phi_j \cdot \overrightarrow{dA}\,|_{ip1} > 0
\end{aligned} \tag{22}$$

Inserting Eqs. (20) and (21) into Eq. (6), the following equation for each element is obtained:

$$Acc_{m,i} + F_{m,i} + q_i = 0; \quad m = 1, \ldots, N_v; \quad i = 1, \ldots, n_c + 1 \tag{23}$$

Eq. (23) denotes the conservation for each sub-control volume of each element. Now, it is necessary to assemble the equation of each control volume obtaining the contribution of each sub-control volume that shares the same vertex. This process is similar to the assembling of the stiffness global matrix in the finite element method. Further details can be found in Cordazzo (2004) and Marcondes and Sepehrnoori (2010). Finalizing this section, it is important to mention that each element can have different permeabilities and porosities, allowing in this way, the simulation of high anisotropic reservoirs.

## 4. Test problems

This section presents four simulation case studies using the EbFVM approach. The first case study was used to validate the implementation of each one of the four element types used to model the reservoir geometry. The results of this case study are validated with the GPAS simulator using Cartesian meshes. Case 1 is the simulation of six-component gas injection in a quarter-of-five spot with the simultaneous flow of gas and oil. Fig. 2 presents the four-refined grid configurations used for this case. It is worthwhile to mention that although the meshes presented in Fig. 1 look alike, they are completely different. In Fig. 2a each block is a hexahedron element, in 'b' each hexahedron is divided in six tetrahedrons, in 'c' each hexahedron is divided in two prisms, and in 'd' each hexahedron is divided in six pyramids, with the apex located at the center of the block. Table 1 presents the fluid and physical properties. As we can see from Table 1, an isotropic and homogeneous reservoir was considered. The relative permeability data for Corey's model is given in Table 2.

The second case study also refers to gas injection in a quarter-of-five spot, but now an anisotropic and heterogeneous reservoir has been considered. Except for the porosity and absolute permeability field, all of the previous data presented for Case 1 were used. The $K_{yy}$ component of the absolute permeability and porosity is presented in Fig. 3. The $K_{xx}$ component was set equal to $K_{yy}$ component, $K_{zz}$ component was set equal to one-tenth of the $K_{xx}$ component, and the other components were set to zero.

In order to present the three hydrocarbon phase capabilities of GPAS simulator, the third case study refers to a fluid flow simulation of three hydrocarbon phases in equilibrium (two liquid

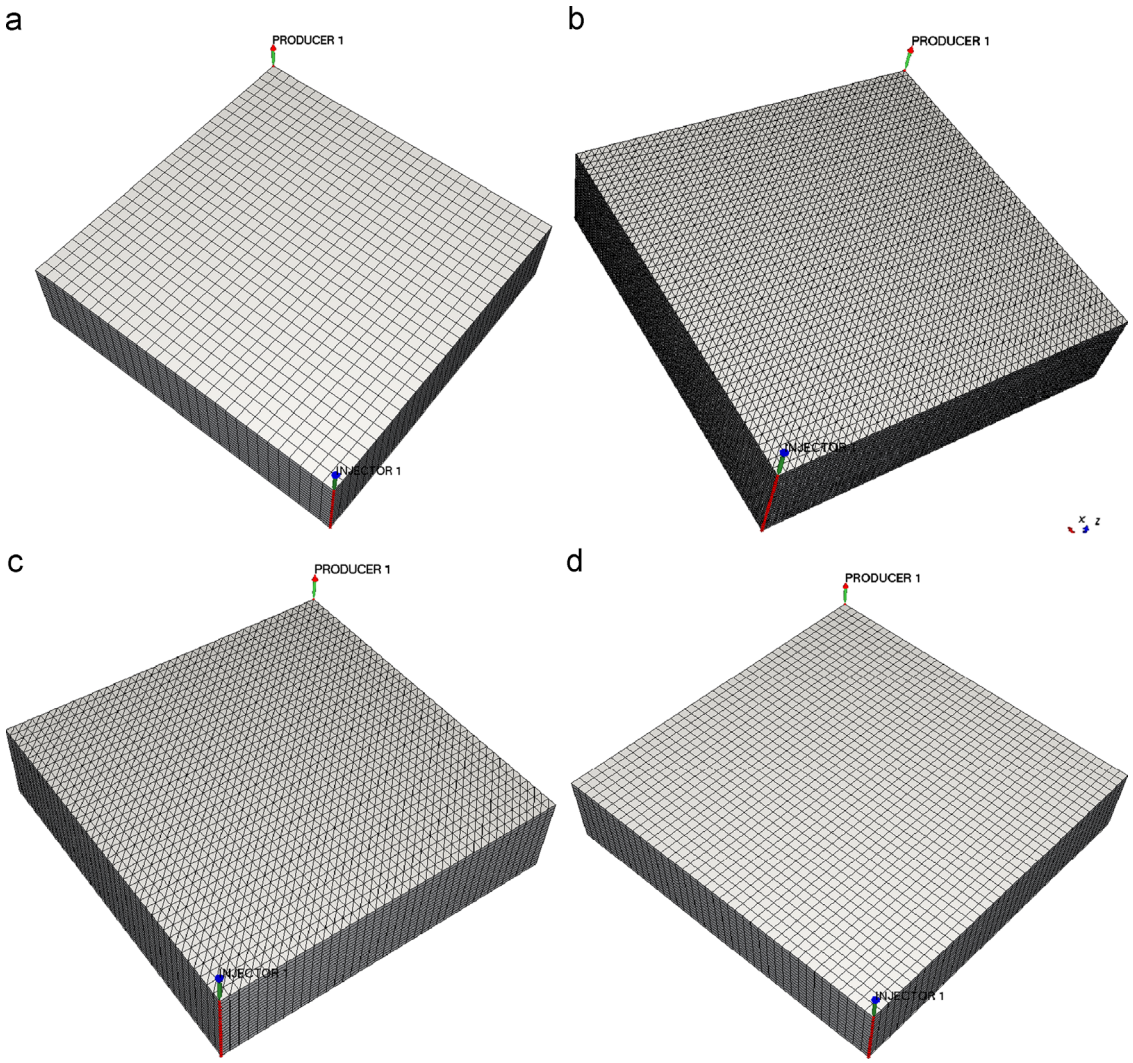


**Fig. 2.** Grid configurations for Case study 1: (a) hexahedron (14,400 elements; 16,337 vertices), (b) tetrahedron (375,000 elements; 67,626 vertices), (c) prism (64,000 elements; 35,301 vertices), and (d) pyramid (153,600 elements; 54,177 vertices).

**Table 1**
Input data for Case 1.

| Reservoir data | Initial conditions | Physical properties and well conditions |
|---|---|---|
| Reservoir dimension ($L_x=L_y=170.69$ m, $L_z=30.48$ m) | Water saturation $S_{wi}=0.17$ | Water viscosity $=1\times10^{-3}$ Pa s<br>Gas injection rate $=0.32774$ m$^3$/s ($10^6$ ft$^3$/d) |
| Absolute permeability ($K_{xx}=K_{yy}=K_{zz}$)$=1.0\times10^{-14}$ m$^2$ (10 mD) | Reservoir pressure $=10.34$ MPa (1500 psi) | Bottom hole pressure $=8.96$ MPa (1300 psi) |
| Porosity $=0.35$ | Overall fraction of hydrocarbon components ($C_1$, $C_3$, $C_6$, $C_{10}$, $C_{15}$, $C_{20}$)$=0.5$, 0.03, 0.07, 0.2, 0.15, 0.05 | Injected mole fraction ($C_1$, $C_3$, $C_6$, $C_{10}$, $C_{15}$, $C_{20}$)$=0.77$, 0.20, 0.01, 0.01, 0.005, 0.005 |

**Table 2**
Corey's model relative permeability data.

| | Water | Oil | Gas |
|---|---|---|---|
| End point relative permeability | 0.4 | 0.9 | 0.9 |
| Residual saturation | 0.3 | 0.1 | 0.0 |
| Exponent of relative permeability | 3.0 | 2.0 | 2.0 |

phases and a gas phase). The reservoir again refers to a gas injection in a quarter-of-five spot. Tables 3 and 4 present the fluid and physical properties, and the relative permeability data for Corey's model, respectively.

The last case study refers to a simulation of a gas injection in an irregular reservoir. Except for the reservoir dimension and absolute permeabilities, we used the same properties shown in Tables 1 and 2. Fig. 4 shows two grid-configurations employed for this reservoir. The first mesh, Fig. 4a, is composed only of hexahedrons, while the other one, Fig. 4b, is a hybrid mesh composed of tetrahedron, pyramid and hexahedron elements. In Fig. 4a and b, we show the reservoir top and bottom topologies, respectively. From these figures, we can see that this reservoir is irregularly shaped in all directions. The absolute permeabilities in the $x$ and $y$ directions were $1.0\times10^{-13}$ m$^2$ (100 mD), and the absolute permeability in the $z$ direction was $1.0\times10^{-14}$ m$^2$ (10 mD). For each injection well, we used the volumetric rate presented in Table 1.

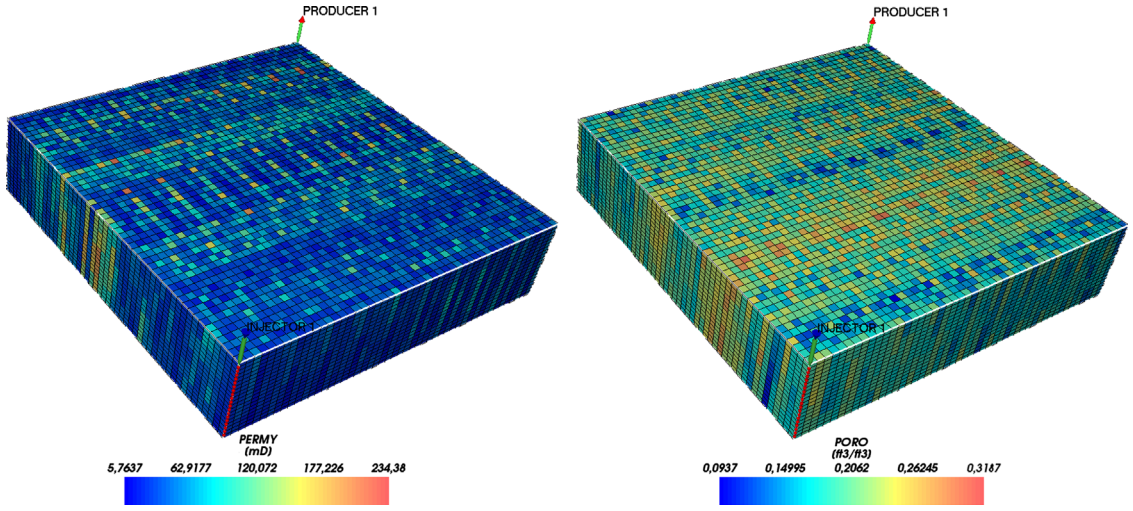


**Fig. 3.** Absolute permeability and porosity data used for Case 2.

**Table 3**
Input data for Case 3.

| Reservoir data | Initial conditions | Physical properties and well conditions |
|---|---|---|
| Reservoir dimension ($L_x=L_y=170.69$ m, $L_z=30.48$ m) | Water saturation $S_{wi}=0.25$ | Water viscosity $=1\times10^{-3}$ Pa s<br>Gas injection rate $=0.32774$ m$^3$/s ($10^6$ ft$^3$/d) |
| Absolute permeability ($K_{xx}=K_{yy}=K_{zz}$) $=1.0\times10^{-13}$ m$^2$ (100 mD) | Reservoir pressure $=6.21$ MPa (900 psi) | Bottom hole pressure $=6.21$ MPa (900 psi) |
| Porosity $=0.30$ | Overall fraction of hydrocarbon components ($CO_2$, $C_1$, $NC_{16}$)$=$ 0.01, 0.19, 0.80 | Injected mole fraction ($CO_2$, $C_1$, $NC_{16}$)$=0.95$, 0.05, 0.00 |

**Table 4**
Corey's model relative permeability data for Case 3.

| | Water | Oil | Gas | Second oil |
|---|---|---|---|---|
| End point relative permeability | 0.3 | 0.75 | 0.9 | 0.9 |
| Residual saturation | 0.25 | 0.2 | 0.0 | 0.0 |
| Exponent of relative permeability | 3.0 | 2.0 | 2.0 | 2.0 |

## 5. Results

Fig. 5 presents the results in terms of volumetric rate at standard conditions for oil, and gas phases for case 1 using all the four implemented elements. The results of this simulation using the GPAS simulator in conjunction with Cartesian grids are also shown. Fig. 5 shows that the results of the present work using a Hexahedron ($30\times30\times16$—14,400 elements; 16,337 vertices), a tetrahedron ($50\times50\times25$—375,000 elements; 67,626 vertices), a prism ($40\times40\times20$—64,000 elements; 35,301 vertices), and pyramid ($40\times40\times16$—153,600 elements; 54,177 vertices) mesh are very close for both oil and gas rates. We can also infer that the number of vertices of pyramid and tetrahedron elements is much larger compared to the hexahedron and prism elements. It is important to mention that the number of vertices is equal to the number of control volumes. The number of vertices of tetrahedron mesh is about 3.16 times larger than the number of vertices of hexahedron mesh. As mentioned by Maliska (2012), the numerical errors mainly of tetrahedron, prism, and pyramids elements cannot be classified as grid orientation effect, since these elements are randomly orientated along the domain. The errors exist, but they cannot be classified as grid orientation errors. We also can verify that the number of control volumes of the coarse Cartesian mesh is about 5.5 times larger than the hexahedron grid.

The results in terms of volumetric rates of oil and gas rates at standard conditions obtained for Case 2 are shown in Fig. 6. This case again refers to a characterization of six hydrocarbon components into a quarter of a five-spot. However, an anisotropic and heterogeneous reservoir has been taken into account. Again, the results obtained in conjunction with the EbFVM for each one of the four types of elements are very close to each other for both oil and gas rates. The gas saturation obtained with the hexahedron element in two simulation times is presented in Fig. 7. Due to the heterogeneity in porosity and permeability, the saturation field is completely asymmetric at the initial stage of the injection process. Later on, that effect disappears due to the increase of saturation field.

The results for Case 3, the three hydrocarbon phase, homogeneous, and isotropic reservoir, in terms of volumetric rates at standard conditions of oil and gas obtained in conjunction with hexahedron element are shown in Fig. 8. The results obtained with GPAS in conjunction with Cartesian are also shown. From Fig. 8, we can observe the volumetric rates of the hexahedron mesh are close to the ones obtained with the Cartesian meshes, specially the more refined one. The spikes present in the curves are due to the phase change along the reservoir associated with the phase composition and pressure changes.

Fig. 9 presents the results, in terms of oil and gas volumetric rates at standard condition, for the last case study in conjunction with the two meshes shown in Fig. 4. Although the two grid configurations are different, the results in terms of oil and gas rates for both grids are in good agreement. The gas saturation field, during two simulation times, is shown in Fig. 10, for the two grid configurations. From this figure, it is possible to observe a good agreement of the saturation field for both grid configurations investigated.

## 6. Conclusions

An element-based finite volume approach for 3D compositional reservoir simulation using unstructured grids based on tetrahedron,

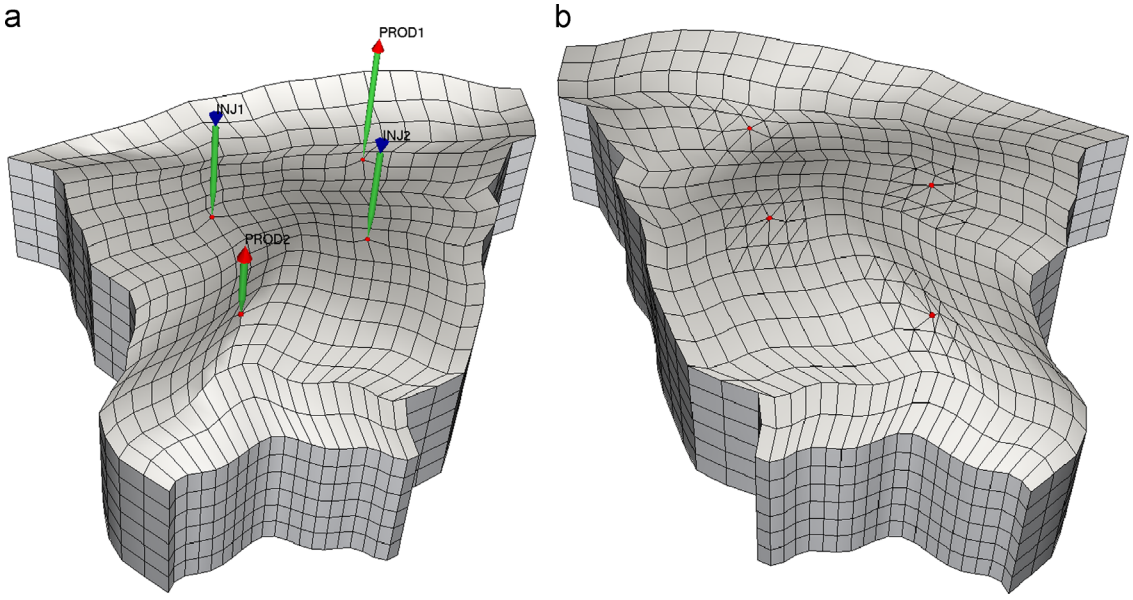


**Fig. 4.** Grid configurations used for Case 4: (a) hexahedron mesh (3087 vertices; 2400 elements) and (b) hybrid mesh (3475 vertices; 3086 tetrahedrons; 1632 hexahedron; 1925 pyramids).

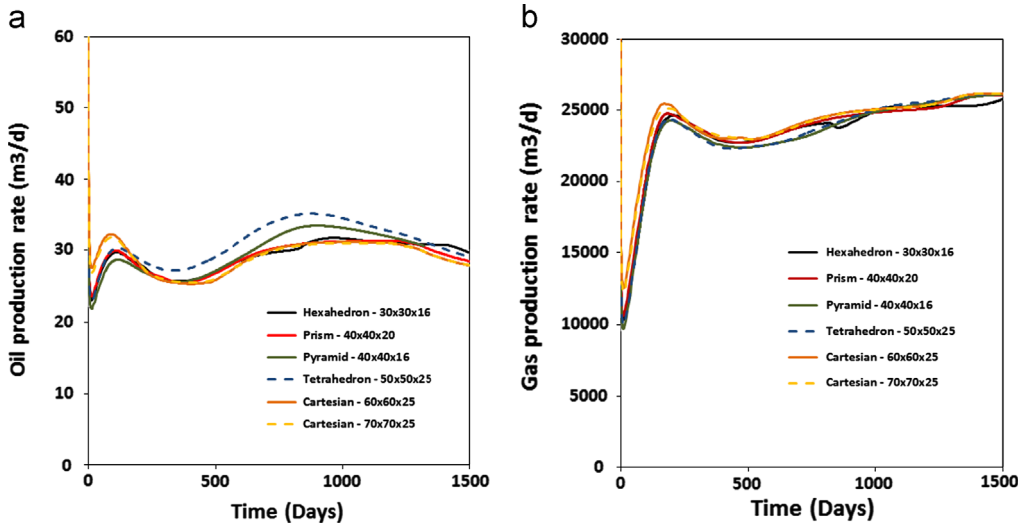


**Fig. 5.** Results for Case 1: (a) oil production rate vs. time and (b) gas production rate vs. time.

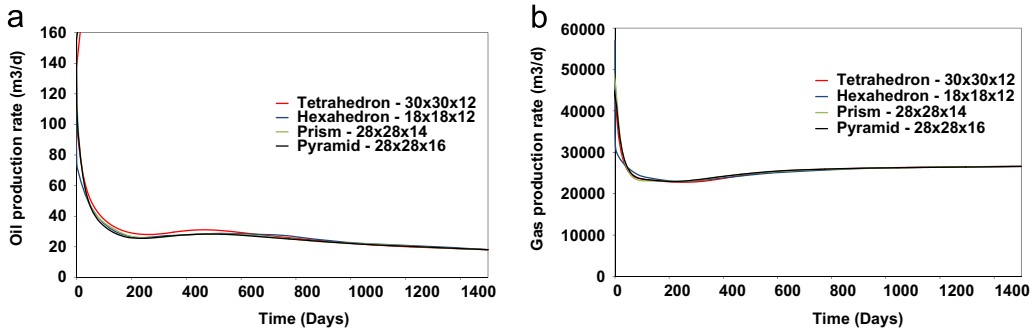


**Fig. 6.** Results for Case 2: (a) oil production rate vs. time and (b) gas production rate vs. time.

prism, pyramid, and hexahedron elements was presented. The results for the gas flooding simulation using the mentioned elements were compared to the results of the original formulation of the GPAS simulator in conjunction with Cartesian meshes. The results of GPAS using fine Cartesian meshes were close to that obtained using the EbFVM approach implemented and tested in the present work. Based

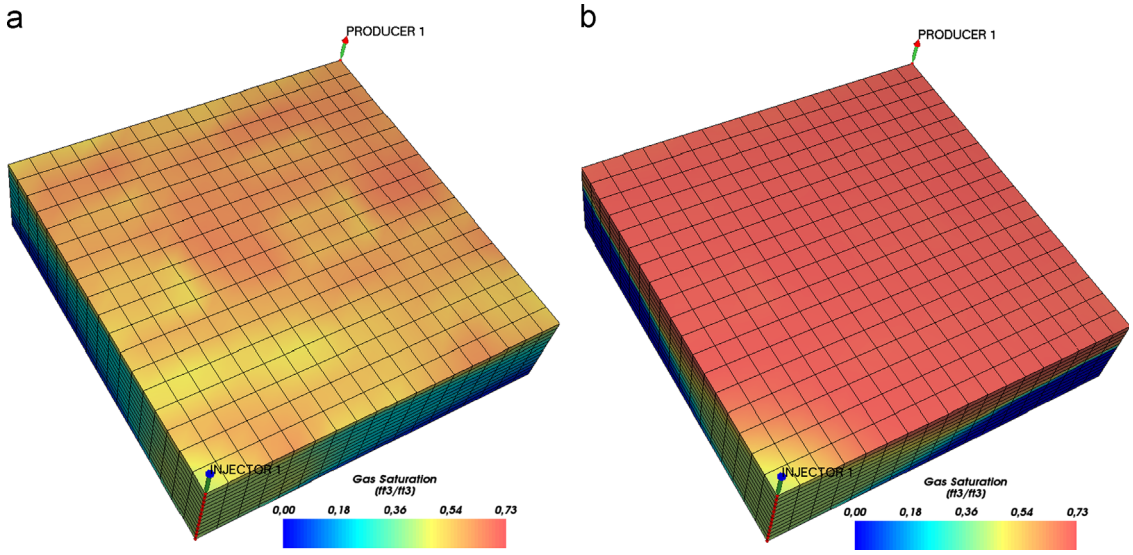


**Fig. 7.** Gas saturation field—hexahedron grid: (a) 80 days and (b) 1001 days.

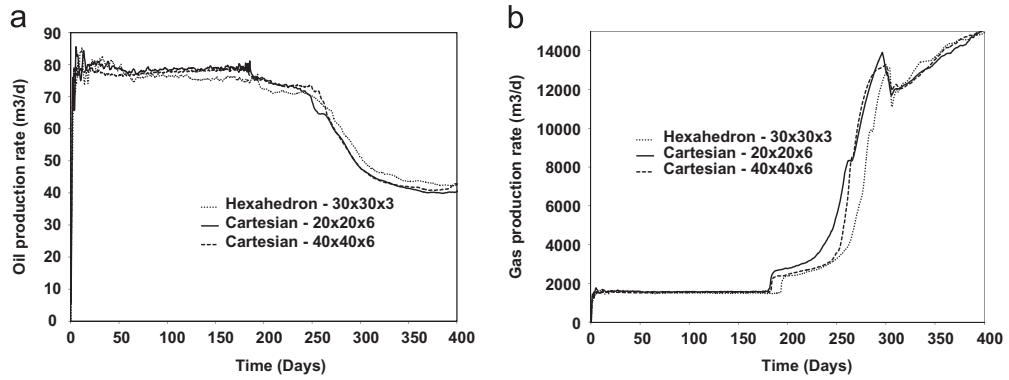


**Fig. 8.** Results for Case 3: (a) oil production rate vs. time and (b) gas production rate vs. time.

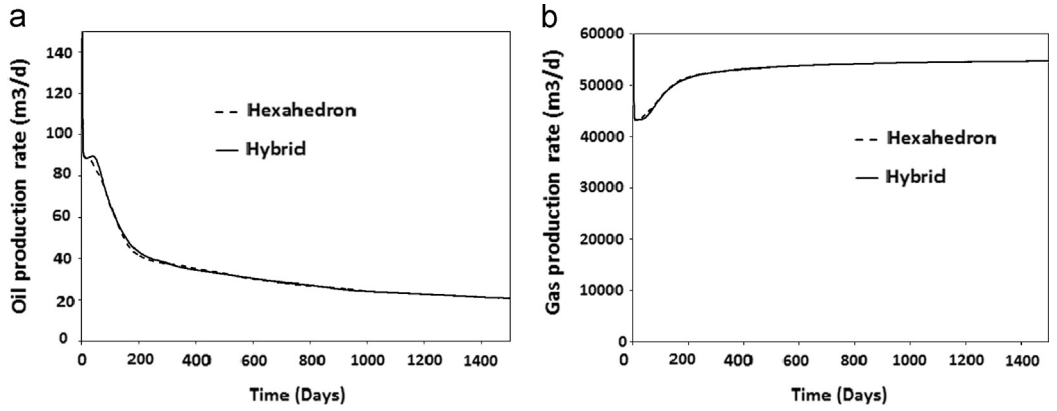


**Fig. 9.** Results for Case 4: (a) oil production rate vs. time and (b) gas production rate vs. time.

on the results presented in this work, the EbFVM method was less prone to the grid orientation effect, but according to the results presented, it can be verified that the numerical error produced by tetrahedron and pyramid elements is larger than by the hexahedron and prism elements. When these results were compared to the ones obtained using GPAS Cartesian grids, it was observed that the simulation using Cartesian grids requires many more gridblocks than the EbFVM approach. In conclusion, the EbFVM approach was tested for several complex reservoir simulation problems and based on the results presented the method was shown to be an excellent method for solving such problems.

## Acknowledgments

This work was conducted with the support of the Reservoir Simulation Joint Industry Project, a consortium of operating and service companies at the Center for Petroleum and Geosystems

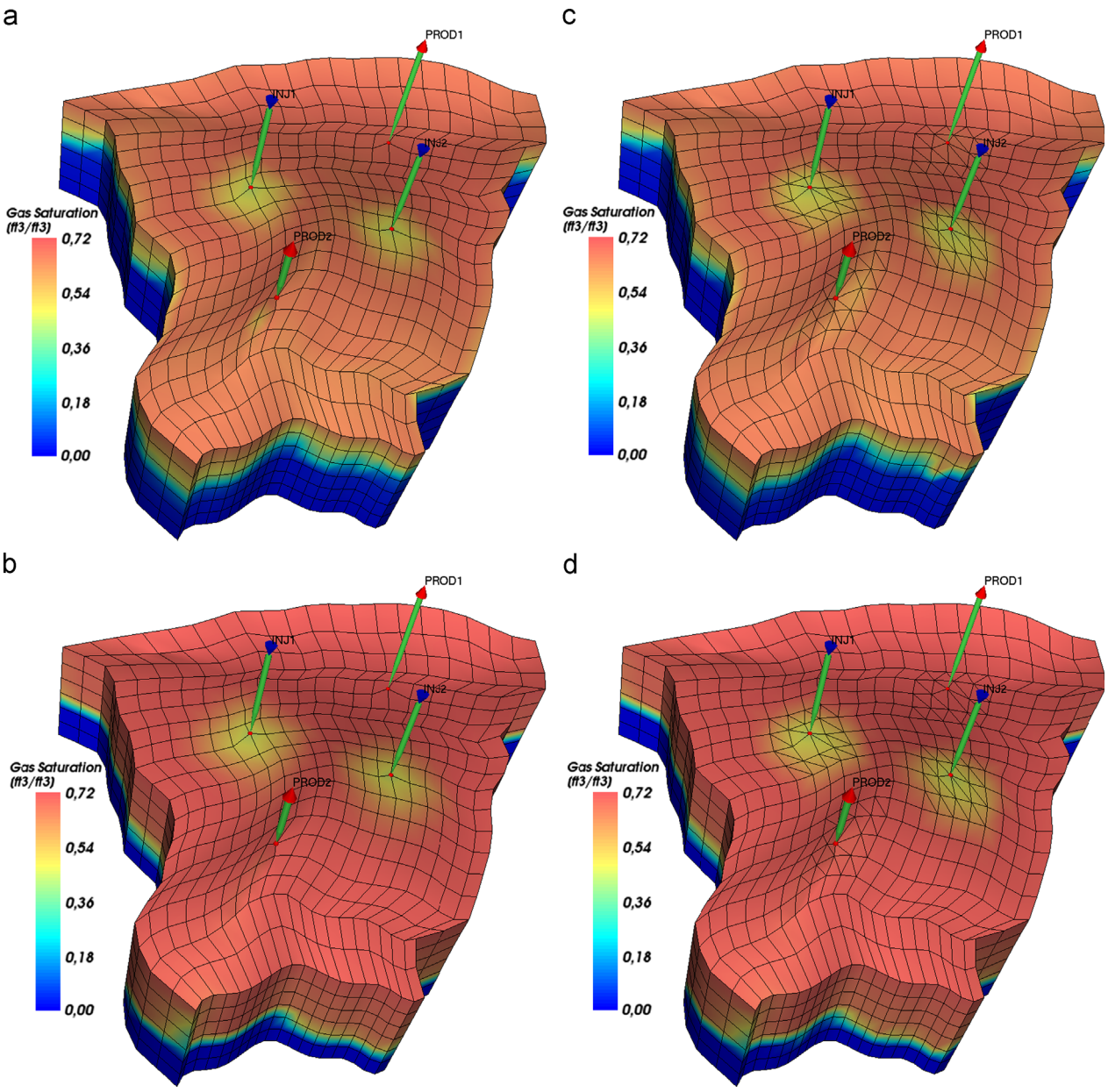


**Fig. 10.** Gas saturation field—Case study 4. Hexahedron: (a) 80 days, (b) 1000 days. Hybrid: (c) 80 days, (d) 1000 days.

Engineering at The University of Texas at Austin. Also, the first author would like to thank CNPq (The National Council for Scientific and Technological Development of Brazil) for their financial support.

## References

Baliga, B.R., Patankar, S.V., 1983. A control volume finite-element method for two-dimensional fluid flow and heat transfer. Numer. Heat Transfer 6, 245–261.

Cordazzo, J., 2004. An element based conservative scheme using unstructured grids for reservoir simulation. In: SPE International Student Paper Contest, The SPE Annual Technical Conference and Exhibition. Houston, Texas.

Cordazzo, J., Maliska, C.R., Silva, A.F.C., Hurtado, F.S.V., 2004a. The negative transmissibility issue when using CVFEM in petroleum reservoir simulation —1. Theory. In: Proceedings of the 10th Brazilian Congress of Thermal Sciences and Engineering—ENCIT 2004, November 29–December 03. Brazilian Society of Mechanical Sciences and Engineering—ABCM, Rio de Janeiro, Brazil.

Cordazzo, J., Maliska, C.R., Silva, A.F.C., Hurtado, F.S.V., 2004b. The negative transmissibility issue when using CVFEM in petroleum reservoir simulation—2. Results. In: Proceedings of the the 10th Brazilian Congress of Thermal Sciences and Engineering—ENCIT 2004, November 29–December 03. Brazilian Society of Mechanical Sciences and Engineering—ABCM, Rio de Janeiro, Brazil.

Deb, M.K., Reddy, M.P., Thuren, J.B., Adams, W.T., 1995. A new generation solution adaptive reservoir simulator. In: The SPE Annual Technical Conference & Exhibition, October, 22–25. Paper SPE 30720. Dallas, TX.

Durlofsky, L.J., Chien, M.C.H., 1993. Development of a mixed finite-element-based compositional reservoir simulator. In: The 12th SPE Symposium on Reservoir Simulation, February 28–March 3. Paper SPE 25253. New Orleans, LA.

Edwards, M.G., 2000. M-matrix flux splitting for general full tensor discretization operators on structured and unstructured grids. J. Comput. Phys. 160, 1–28.

Edwards, M.G., 2002. Unstructured, control-volume distributed, full-tensor finite-volume schemes with flow based grids. Comput. Geosci. 6, 433–452.

Forsyth, P.A., 1990. A Control-Volume, Finite-Element Method for Local Mesh Refinement in Thermal Reservoir Simulation. SPE Paper 18415, November, pp. 561–566.

Fung, L.S., Hiebert, A.D., Nghiem, L., 1991. Reservoir simulation with a control-volume finite-element method. In: The 11th SPE Symposium on Reservoir Simulation, February 17–20. Paper SPE 21224. Anaheim, California.

Gottardi, G., Dall´Olio, D., 1992. A control-volume finite-element model for simulating oil–water reservoirs. J. Pet. Sci. Eng. 8, 29–41.

Hegre, T.M., Dalen, V., Henriquez, A., 1986. Generalized transmissibilities for distorted grids. In: Proceedings of the 61st Annual Technical Conference and Exhibition of the Society of Petroleum Engineers, October 5–8. Paper SPE 15622. New Orleans, LA.

Hoteit, H., Firoozabadi, A., 2005. Multicomponent fluid flow by discontinuous Galerkin and mixed methods in unfractured and fractured media. Water Resour. Res. 41, 1–15.

Hoteit, H., Firoozabadi, A., 2006. Compositional modeling by the combined discontinuous Galerkin method and mixed methods. SPE J. 11, 19–34.

Hughes, T.J.R., 1987. The Finite Element Method, Linear Static and Dynamic Finite Element Analysis. Prentice Hall, New Jersey.

Maliska, C.R., 2004. Heat Transfer and Computational Fluid Mechanics, 2nd ed. Editora LTC, Florianópolis. (in Portuguese).

Maliska, C.R., 2012. Personal communication.

Marcondes, F., and Sepehrnoori, K., 2007. Unstructured grids and an element based conservative approach for compositional reservoir simulation. In: Proceedings of the 19th International Congress of Mechanical Engineering, November 5–9. Brasília, DF, Brazil.

Marcondes, F., Sepehrnoori, K., 2010. An element-based finite-volume method approach for heterogeneous and anisotropic compositional reservoir simulation. J. Pet. Sci. Eng. 73, 99–106.

Paluszny, A., Matthäi, Hohmeyer, M., 2007. Hybrid finite element-finite volume discretization of complex geologic structures and a new simulation workflow demonstrated on fractured rocks. Geofluids 7, 168–208.

Parashar, M., Wheeler, J.A., Pope, G., Wang, K., Wang, P., 1997. A new generation EOS compositional reservoir simulator: part II—framework and multiprocessing. In: SPE Reservoir Simulation Symposium. Paper SPE 37977. Dallas, USA.

Raw, M., 1985. A New Control Volume Based Finite Element Procedure for the Numerical Solution of the Fluid Flow and Scalar Transport Equations. University of Waterloo, Waterloo, Ontario, Canada. (Ph.D. thesis).

Verma, S., Aziz, K., 1997. A control volume scheme for flexible grids in reservoir simulation. In: The Reservoir Symposium. Paper SPE 37999. Dallas, Texas, pp. 8–11.

Wang, P., Yotov, I., Wheeler, M., Arbogast, T., Dawson, C., Parashar, M., Sepehrnoori, K., 1997. A new generation EOS compositional reservoir simulator: part I—formulation and discretization. In: SPE Reservoir Simulation Symposium. Paper SPE 37079. Dallas, Texas.